Performance of the Pierre Auger Fluorescence Detector at the highest energies

Viviana Scherini
Department of Physics, Bergische Universität Wuppertal, D-42097 Wuppertal, Germany
for the Pierre Auger Collaboration
Email: scherini@physik.uni-wuppertal.de

***Abstract*— The hybrid detector of the Pierre Auger Observatory has been designed to measure extensive air showers induced by cosmic rays of energies up to 10^{21} eV. A detailed study of the Fluorescence Detector response to very high energy simulated events has been done in order to check its performance. A new technique has been implemented to improve the capability of the full simulation-reconstruction chain at the highest energies.**

I. Introduction

The fluorescence detector (FD) of the Pierre Auger Observatory is currently operating 18 fluorescence telescopes of the 24 that will be employed in the completed detector. These telescopes, grouped in 4 eyes each consisting of 6 telescopes, measure the longitudinal profile of cosmic ray showers with a 10 to 15% duty cycle. The FD reconstruction capability has been studied using a complete simulation and reconstruction production chain, see also [1]. The focus of this study has been placed in particular on its performances at the highest energies. A detailed description of the FD simulation program, reconstruction framework is given in [2] and [3].

A. Generation parameters and reconstruction requirements

The simulation sample consists of CORSIKA [4] showers, 4400 proton and 4150 iron showers, with fixed zenith angles of 0°, 18°, 26°, 37°, 45°, 60° and energies ranging between $10^{17.5}$ and 10^{21} eV in steps of 0.5 in the logarithmic scale. The showers have been generated with the core positions in a slice of 2° in the field of view of Los Leones Eye Bay 4, with uniformly distributed core distances (see Fig. 1). Assumptions for the atmosphere, detector calibration and fluorescence yield calculation have been made consistently throughout the simulation-reconstruction chain.
For a detailed study of the detector response at the highest energies, including the FD saturation region, the proton set has been re-sampled at core distances of 5, 10, 15, 20 and 25 km from the eye, for a total of 22000 showers.
In this study, the FD resolution in energy and depth of the shower maximum has been estimated for the case of known fixed shower geometry, namely the true geometry has been given as input to the shower reconstruction algorithm. Setting the geometry to the true value provides a fairly realistic estimate of the detector resolution for the hybrid mode. This assumption is justified by the argument that hybrid reconstruction benefits from a more accurate shower geometry with respect to the monocular fluorescence reconstruction.

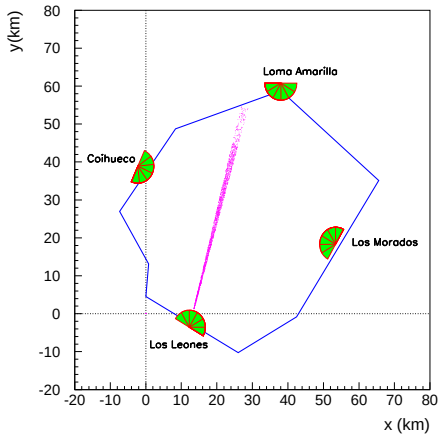

Fig. 1. A sketch of the Pierre Auger Observatory showing the core positions of the simulated showers. The showers have been generated in a slice of 2° in the fi eld of view of Los Leones Eye Bay 4, with uniformly distributed core distances

A description of the hybrid performance of the Pierre Auger Observatory is given in [5].

In order to focus on ”reconstructible” events only, the observed profile and reconstructed shower depth at maximum are required to satisfy the following conditions:

- successful Gaisser-Hillas fit for the longitudinal shower profile with $\chi^2/\mathrm{Ndof} < 5$
- observed longitudinal shower profile wider than 200 g/cm^2
- fitted $X_{\max}$ position located in the field of view.

The method adopted here for the reconstruction of longitudinal shower profiles and shower energies with the Auger Fluorescence telescope is described in [6].

II. Energy and $X_{\max}$ resolution

The residual of reconstructed depth at shower maximum is shown in Fig. 2(a), top panel, for proton (black line, RMS=25 g/cm^2) and iron (red dot-dashed line, RMS=22 g/cm^2). Fig. 2(b), bottom panel, shows the energy residual distribution for proton initiated events with fixed geometry (blue line) and with reconstructed geometry (red dot-dashed line). The energy resolution improves and the number of reconstructible events is larger by a factor 2 with respect to

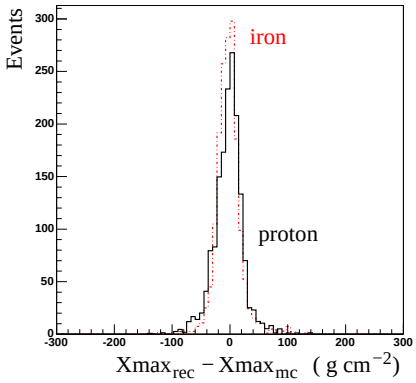

(a)

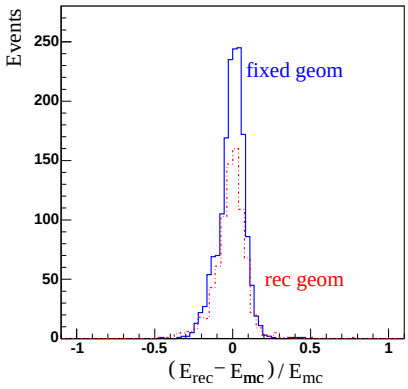

(b)

Fig. 2. (a) Residual distribution of the reconstructed depth at shower maximum (reconstructed $X_{\max}$ - true $X_{\max}$) for proton (black line, RMS=25 g/cm^2) and iron (red dot-dashed line, RMS=22 g/cm^2). (b) Energy resolution for the simulated data sample with true geometry (blue line, 1607 events, RMS=9%) and reconstructed monocular geometry (red dot-dashed line, 798 events, RMS=11%). The values are obtained averaging over the entire sample.

the case of the pure monocular reconstruction. The resolutions shown have been calculated for a clean atmosphere (aerosol horizontal attenuation length at sea level of 24 km and scale height of 2 km) and averaged over the entire sample. Further details on FD reconstruction performance and comparison with data are discussed in [7].

Fig. 3 shows the RMS of the energy residual distribution as a function of shower energy (top), zenith angle (middle) and core distance (bottom), averaged over the entire sample. The error bars include the statistical fluctuations only. The RMS has a stable average value of about 9% over the studied core distance and zenith angle range improving with increasing energy. The on-going study of the detector performance at the highest energies includes also the detector pixellation effect. At energies around $10^{19.5}$ eV the reconstructed profile begins to show a wavy sub-structure due to the inhomogeneity of light collection at the telescope focal surface.

A more detailed model taking into account the necessary corrections to the profile reconstruction algorithm is currently being optimised, see [8]. A first test run on a sample of 200

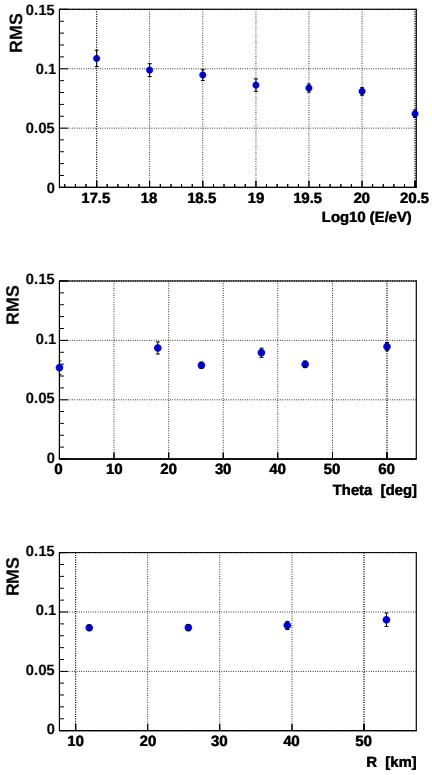

Fig. 3. RMS of the energy residual distribution as a function of true energy (top), zenith angle (middle) and core distance (bottom), averaged on the entire sample. Error bars include the statistical fluctuations only.

showers with energy 10^{21} eV, has been performed including this so called Spot method in the reconstruction algorithm. A common effort to validate the method with dedicated simulations is in progress. Fig. 4 shows the achieved accuracy to be 5.7% (RMS).

III. Covering the largest signal dynamic range

A. The virtual channel working principle

The dynamic range of the recorded signal runs from 3 to almost 10^5 photoelectrons/100ns. The analog electronics have been designed to properly handle a 15 bits dynamic range using 12 bits ADCs, see [9], [10]. Each analog board carries 24 ADC, 22 for the normal channel (high gain), 2 for the virtual channel (low gain). Parallel to the normal readout, the virtual readout records the sum of 11 non adjacent even (or odd) normal channels.

This system is designed to process signals with amplitudes beyond the saturation limit of the normal PMT readout channel. If a normal channel saturates, the information on the signal can be recovered looking at the virtual channel and subtracting time-bin wise the contribution of the not saturated PMTs.

A display of a simulated very high energy event is shown in Fig. 5. On the left a sketch of the FD camera showing the sky view of the light track hitting the PMTs. The color scheme reflects the triggering time (blue earlier, red later). On

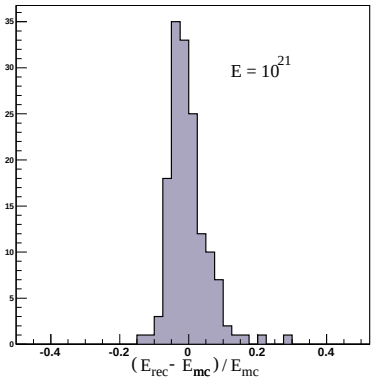

Fig. 4. Energy residual distribution for events at 10^{21} eV including the corrections for light collection inhomogeneity, the so called Spot model, see [8]. Average -0.002, RMS 0.057.

the right the ADC traces for the 5 selected pixels belonging to the same column are displayed. In black the signal in the corresponding virtual channel. Whereas some of the normal signals are saturated the associated virtual channel keeps both amplitude and charge information.

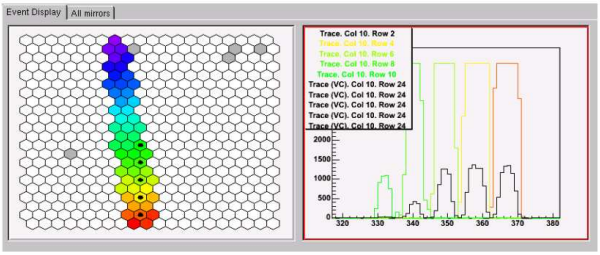

Fig. 5. Display of a simulated very high energy event: on the left the FD camera with the light track hitting the PMTs; the color scheme reflects the trigger time (blue earlier, red later). On the right the ADC traces for the 5 selected pixels. Whereas some of the normal signals are saturated the associated virtual channel keeps both amplitude and charge information.

B. Simulating a very high energy event close to the detector

The virtual channel readout has been implemented in both the simulation and reconstruction algorithms. On the simulation side the normal and virtual ADCs are basically handled setting the two different electronic gains. At the reconstruction stage the signal traces of the hit PMTs are loaded and a check for saturation is performed bin per bin.

If saturation occurs the PMT trace is loaded from the corresponding virtual channel: the affected time bins are replaced with the values from the virtual ADC counts scaled for the relative gain ratio.

Our simulation has shown that, in case of saturation, even vertical showers at short distance from the FD detector, where the whole signal falls into the same virtual channel, could be recovered as the single PMT peaks are time separated.

After saturation recovery the usual conversion to photons at diaphragm is performed and the single traces are combined to

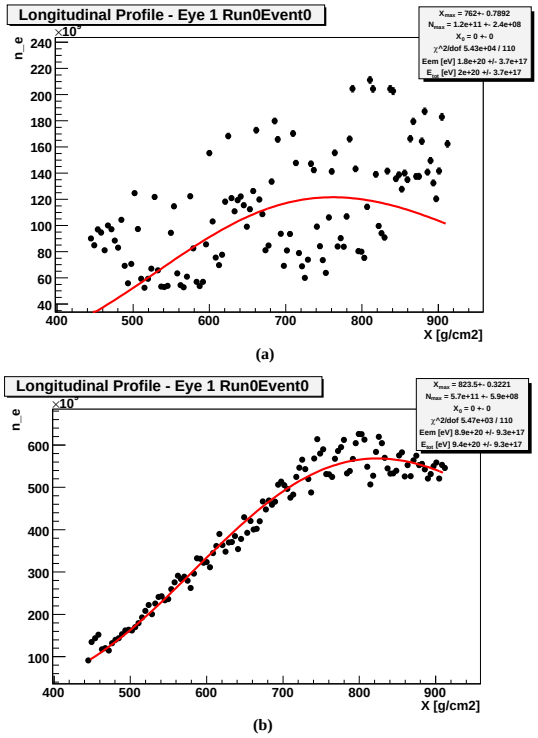

Fig. 6. Reconstructed shower longitudinal profile of an event with energy 10^{21} eV and depth of shower maximum at 825 g/cm^2 : top plot (a) before saturation recovery (fitted energy 1.8x10^{20} eV, fitted $X_{\max}$ 762 g/cm^2); bottom plot (b) after saturation recovery (fitted energy 9.4x10^{20} eV, fitted $X_{\max}$ 824 g/cm^2).

build the light flux and finally the longitudinal shower profile (number of charged particles vs slant depth).

In Fig. 6 an example of a reconstructed profile of an event with energy 10^{21} eV and depth of shower maximum at 825 g/cm^2 is given. The top plot (a) shows the saturated longitudinal profile (fitted energy 1.8x10^{20} eV, fitted $X_{\max}$ 762 g/cm^2), while the bottom plot (b) shows the same profile after saturation recovery (fitted energy 9.4x10^{20} eV, fitted $X_{\max}$ 824 g/cm^2). The shape of the emitted light flux is recovered and a much better agreement between the fitted energy and $X_{\max}$ and the corresponding true value is achieved. Further improvement is expected over the entire sample when the corrections for light collection inhomogeneity will be included.

C. Studying the saturation region

A detailed study of the Fluorescence Detector saturation region based on a sample of very high-energy events placed at different core distances, has been performed in order to quantify the fraction of events saturating the high-gain (normal) channel. The eventuality of saturation in the low-gain (virtual) channel is considered too as it would cause the loss of information on collected charge. A proper setting of the gain ratio has been defined in order to avoid it. This value is now chosen as safe for detector operations and it is nightly monitored via the relative calibration procedures.

Fig. 7 shows, in a energy-distance plot, the fraction of events with at least one saturated pixel in at least one time bin. The

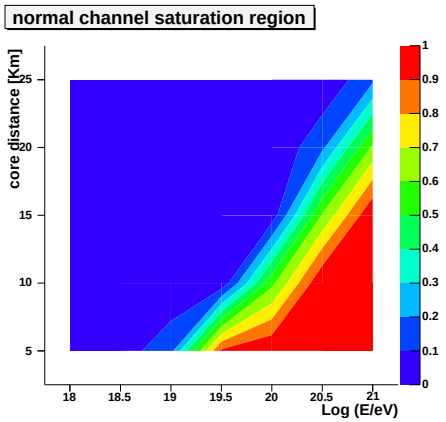

Fig. 7. Fraction of saturated events in the normal readout channel as a function of primary energy and core distance.

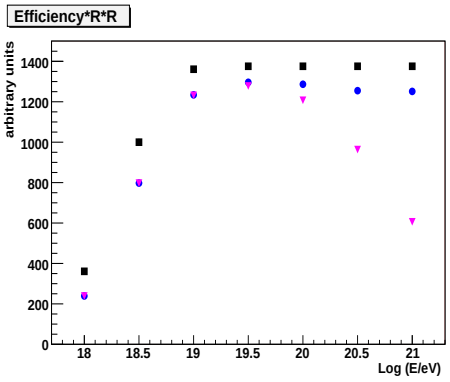

Fig. 8. Detector aperture (arbitrary units) as a function of energy for all the recovered events (black) and for events surviving the reconstruction cuts (blue). Saturated events removed (pink). At the simulated core distances detector effi ciency is 100% already at 19.5 eV.

fraction of saturated events already begins to be significant at short distances for an energy of 10^{19} eV and remains above 50% at higher energies with core distances increasing in steps of 5 km for each half decade in energy. Events like those are in most cases fully recoverable using the virtual readout. Even for the closest events the recovered information is very useful allowing the FD stereo reconstruction.

In Fig. 8 the Fluorescence Detector aperture (in arbitrary units) is plotted as a function of energy for all the recovered events (black), for events surviving the reconstruction cuts (blue) and just removing the saturated events (pink). The flattening of the curve is due to the fact that the maximum core distance in the simulation sample is limited to 25 km where the Fluorescence Detector efficiency is 100% already at energies of 19.5 eV.

IV. Conclusion

The performance of the Auger Fluorescence Detector at the highest energies has been studied using a large number of simulated CORSIKA showers. The energy resolution has been estimated for the case of known fixed shower geometry which provides a fairly realistic estimate for the hybrid operation of the Pierre Auger Observatory. The overall energy resolution depends weakly on the shower energy getting to 5.7% at 10^{21} eV and remains stable with an average value (RMS) of 9% over the studied range of zenith angles (0° - 60°) and core distances (5 - 60 km). The resolution of the atmospheric depth at shower maximum, averaged over the whole sample, is at the level of 22 g/cm^2 for iron and 25 g/cm^2 for protons.

A detailed method correcting for inhomogeneities of light collection on the focal surface has been tested on the highest energy sample where the detector pixellation effect must be taken into account .

Finally the saturation region of the Fluorescence Detector has been studied in detail and the fraction of saturated events, as a function of energy and core distance, has been estimated. Those events can be fully recuperated via the first saturation recovery algorithm, implemented and validated with dedicated simulations.

Acknowledgment

The work was supported by the German Ministry for Education and Research (BMBF). The author would like to thank the Auger Collaboration and especially the Wuppertal group for stimulating discussions and support.

References

[1] A.Ewers, H.Geenen, K-H.Kampert, L.Perrone, S.Robbins, V.Scherini, M.Unger for the Pierre Auger Collaboration, *Validation of the Real and Simulated Data of the Pierre Auger Fluorescence Telescopes*, 29th ICRC, Pune (2005) **7**, 115-118. astro-ph/0507486.
[2] L. Prado Jr. et al., Nucl. Instr. Meth. A 545, 632 (2005)
[3] S. Argirò et al., for the Pierre Auger Collaboration, 29th ICRC, Pune (2005) **8**, 343-346.
[4] D. Heck et al., Report FZKA 6019, (1998).
[5] M. Mostafà for the Pierre Auger Collaboration, 29th ICRC, Pune, India, (2005) **7**, 369-372.
[6] J. Bellido for the Pierre Auger Collaboration, 29th ICRC, Pune (2005) **7**, 13-16.
[7] H.Geenen for the Pierre Auger Collaboration, *Analysis of the Pierre Auger Fluorescence Data*, at this Conference.
[8] P. Facal San Luis, PhD Thesis, *High Energy Cosmic Rays at the Auger Observatory Fluorescence Detector*, Santiago de Compostela (Spain), April 2005.
[9] Pierre Auger Project Technical Design Report, pp 77-84.
[10] S. Argiro et al., Nucl. Instr. Meth. A 461, 440 (2001)